Nanoscale Res Lett (2008) 3:55–59
DOI 10.1007/s11671-007-9114-0

NANO EXPRESS

Theory of Raman Scattering by Phonons in Germanium Nanostructures

Pedro Alfaro-Calderón · Miguel Cruz-Irisson · Chumin Wang-Chen

Received: 24 September 2007 / Accepted: 5 December 2007 / Published online: 21 December 2007

Abstract Within the linear response theory, a local bond-polarization model based on the displacement–displacement Green's function and the Born potential including central and non-central interatomic forces is used to investigate the Raman response and the phonon band structure of Ge nanostructures. In particular, a supercell model is employed, in which along the [001] direction empty-column pores and nanowires are constructed preserving the crystalline Ge atomic structure. An advantage of this model is the interconnection between Ge nanocrystals in porous Ge and then, all the phonon states are delocalized. The results of both porous Ge and nanowires show a shift of the highest-energy Raman peak toward lower frequencies with respect to the Raman response of bulk crystalline Ge. This fact could be related to the confinement of phonons and is in good agreement with the experimental data. Finally, a detailed discussion of the dynamical matrix is given in the appendix section.

Keywords Raman scattering · Phonons · Germanium nanostructures

P. Alfaro-Calderón · M. Cruz-Irisson (✉)
Instituto Politécnico Nacional, ESIME-Culhuacan,
Av. Santa Ana 1000, Mexico 04430, DF, Mexico
e-mail: irisson@servidor.unam.mx

C. Wang-Chen
Instituto de Investigaciones en Materiales,
Universidad Nacional Autónoma de México,
Apartado Postal 70-360, Mexico 04510, DF, Mexico

Introduction

In comparison with silicon (Si) and III–V compounds, germanium (Ge) has a larger dielectric constant and then is particularly suitable for photonic crystal applications. Also, one can incorporate Ge islands into Si-based solar cells for more efficient light absorption. In general, the presence of many arrays of quantum dots with lower bandgap than that of the p–i–n solar cell structure in which they are embedded can lead to an enhancement of the quantum efficiency [1]. Recently, porous Ge (p-Ge) [2–4] and Ge nanowires (GeNW) [5, 6] have been successfully produced and Raman scattering is used to study the phonon behavior in these materials. Although there are many reports about porous Si and Si nanowires, only few investigations have been carried out on Ge nanostructures. However, GeNW hold some special interest in comparison to Si ones, because Ge has, for example, a higher electron and hole mobility than Si, which would be advantageous for high-performance transistors with nanoscale gate lengths.

The reduction of crystallite sizes to nanometer scale can drastically modify the electronic, phononic, and photonic behaviors in semiconductors. Raman scattering, being sensitive to the crystal potential fluctuations and local atomic arrangement, is an excellent probe to study the nanocrystallite effects. Moreover, Raman spectroscopy is an accurate and non-destructive technique to investigate the elementary excitations as well as the details of microstructures. For example, the line position and shape of Raman spectra may give useful information of crystallinity, amorphicity, and dimensions of nanoscale Ge.

In this article, we report a theoretical study of the Raman response in Ge nanostructures by means of a local polarization model of bonds, in which the displacement–displacement Green's function, the Born potential

including central and non-central forces, and a supercell model are used. This model has the advantage of being simple and providing a direct relationship between the microscopic structure and the Raman response.

Modeling Raman Scattering

Raman scattering analysis is a very powerful tool for studying the composition, bonding, and microstructure of a solid. However, the elementary excitation processes involved are complicated to describe theoretically. In general, the Raman response depends on the local polarization of bonds due to the atomic motions. Considering the model of the polarizability tensor developed by Alben et al. [7], in which the local bond polarizabilities [α (j)] are supposed to be linear with the atomic displacements $u_\mu(j)$, i.e., $c_\mu(j) = \partial\alpha(j)/\partial u_\mu(j)$ alternates only in sign from site to site in a single crystal with diamond structure, the Raman response [$R(\omega)$] at zero temperature could be expressed within the linear response theory as [8, 9].

$$R(\omega) \propto \omega \, \mathrm{Im} \sum_{\mu,\,\mu'} \sum_{i,\,j} (-1)^{i-j} G_{\mu,\,\mu'}\,(i,\,j,\,\omega), \tag{1}$$

where μ, $\mu' = x$, y, or z, i and j are the index of atoms, and $G_{\mu,\,\mu'}\,(i,\,j,\,\omega)$ is the displacement–displacement Green's function determined by the Dyson equation as

$$(M\omega^2\mathbf{I} - \mathbf{\Phi})\,\mathbf{G}(\omega) = \mathbf{I}, \tag{2}$$

where M is the atomic mass of Ge, $\mathbf{I}$ stands for the identity matrix, and $\mathbf{\Phi}$ is the dynamical matrix, whose elements are given by

$$\Phi_{\mu\mu'}(i,\,j) = \frac{\partial^2 V_{ij}}{\partial u_\mu(i)\partial u_{\mu'}(j)}. \tag{3}$$

Within the Born model, the interaction potential (V_{ij}) between nearest-neighbor atoms i and j can be written as [10].

$$V_{ij} = \frac{\alpha-\beta}{2}\left\{[\mathbf{u}(i) - \mathbf{u}(j)]\cdot\hat{\mathbf{n}}_{ij}\right\}^2 + \frac{\beta}{2}[\mathbf{u}(i) - \mathbf{u}(j)]^2, \tag{4}$$

where $\mathbf{u}(i)$ is the displacement of atom i with respect to its equilibrium position, α and β are, respectively, central and non-central restoring force constants. The unitary vector $\hat{\mathbf{n}}_{ij}$ indicates the bond direction between atoms i and j. The dynamical matrix within the Born model is described in details in Appendix A.

Results

In order to determine the parameters of the Born model for Ge, we have performed a calculation of the phonon band structure for crystalline Ge (c-Ge) using $\alpha = 0.957$ N cm^{-1} and $\beta = 0.244$ N cm^{-1}, and the results are shown in Fig. 1a. Notice that the optical phonon bands are reasonably reproduced in comparison with the experimental data [11], since these optical phonon modes are responsible for the Raman scattering. It is worth mentioning that these parameter values are very close to those used in a generalized Born model for c-Ge [12]. The Raman response of c-Ge obtained from Eq. 1 is shown in Fig. 1b. Observe that the Raman peak is located at $\omega_0 = 300.16$ cm^{-1} [13, 14], which corresponds to the highest-frequency of optical modes with phonon wave vector $\mathbf{q} = \mathbf{0}$, since the $\mathbf{q}$ of the visible light is much smaller than the first Brillouin zone and then the momentum conservation law only allows the participation of vibrational modes around the Γ point.

The p-Ge is modeled by means of the supercell technique, in which columns of Ge atoms are removed along the [001] direction [15]. In Fig. 2, the highest-frequency Raman shift (ω_R) is plotted as a function of the porosity for square pores, increasing the size of supercells and maintaining the thickness of two atomic layers in the skeleton. The porosity is defined as the ratio of the removed Ge-atom number over the original number of atoms in the supercell. In Fig. 2, we have removed 18, 50, 98, 162, 242, and 338 atoms from supercells of 32, 70, 128, 200, 288, and 392 atoms, respectively. Observe that the results of ω_R are close to 270 cm^{-1}, instead of 300.16 cm^{-1} for c-Ge, due to the phonon confinement originated by extra nodes in the wavefunctions at the boundaries of pores. However, this confinement is only partial since the phonons still have extended wave functions, and the Raman shifts in Fig. 2 are mainly determined by the degree of this partial confinement. The inset of Fig. 2 illustrates the highest-frequency Raman peak and the corresponding p-Ge structure with a porosity of 56.25%.

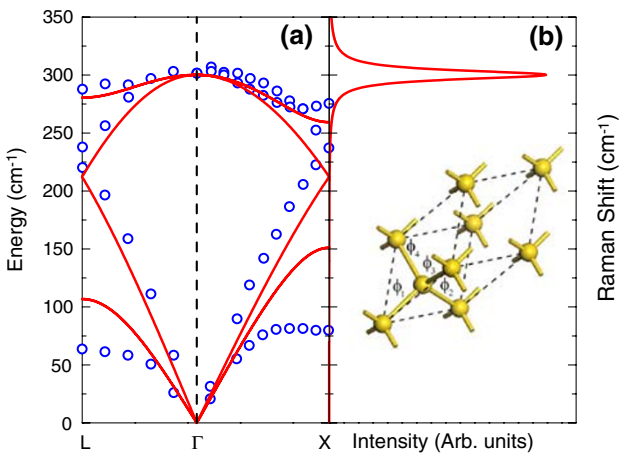

Fig. 1 (**a**) Calculated phonon dispersion relations (*solid line*) compared with experimental data (*open circle*). (**b**) Raman response of c-Ge obtained from a primitive unitary cell, as illustrated in the inset

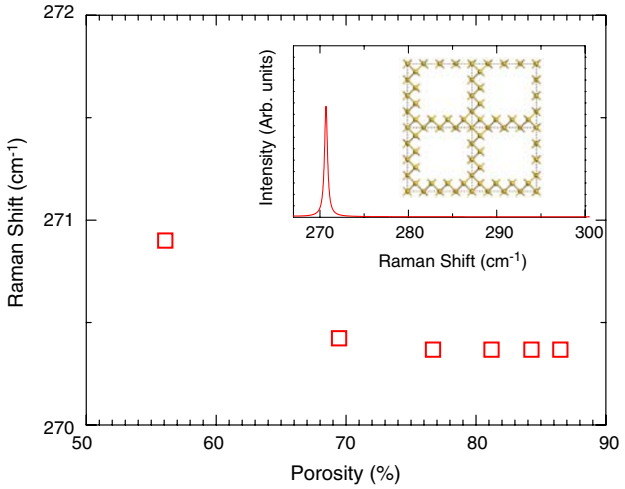

Fig. 2 Variation of Raman peaks as a function of porosity for the square-pore case. Inset: The main Raman peak for p-Ge with a porosity of 56.25%, which corresponds to a supercell of 32 Ge atoms, removing 18 of them

Another way to produce pores consists in removing different number of atoms from a fix large supercell. In this work, we start from a c-Ge supercell of 648 atoms formed by joining 81 eight-atom cubic supercells in the x–y plane. Columnar pores with rhombic cross-section are produced by removing 4, 9, 25, 49, 81, 121, 169, 225, and 289 atoms, as schematically illustrated in the upper inset of Fig. 3 for a pore of 121 atoms. The results of ω_R are shown in Fig. 3 as a function of porosity. In the lower inset of Fig. 3, we present the variation of ω_R with respect to its crystalline Raman peak ω_0, i.e., $\Delta\omega \equiv \omega_0 - \omega_R$, as a function of the inverse of partial confinement distance between pore boundaries (d) in a log–log plot. Observe that for the high-porosity regime (small d) the slope tends to two, similar to the electronic case [16].

For modeling GeNW, we start from a cubic supercell with eight Ge atoms, and take the periodic boundary condition along z-direction and free boundary conditions in x and y directions. For GeNW with larger cross-sections, Ge atomic layers are added in x and y directions to obtain GeNW with different shapes of cross-section. We have performed the calculation of the Raman response for GeNW, whose supercells containing from 8 to 648 Ge atoms. In Fig. 4, ω_R is plotted as a function of the length (L) of cross-sections with square (open squares), rhombic (open rhombus), and octagonal (open circles) forms. These results are compared with experimental data (solid square) obtained from Ref. [14], observing a good tendency agreement. The inset shows $\Delta\omega \equiv \omega_0 - \omega_R$ as a function of $1/L$. Observe that $\Delta\omega \sim L^{-\nu}$ with ν is 1.4–2.0 when $L \to 0$. This result is in agreement with the effective mass theory, i.e., $2L$ is the longest wavelength in x and y directions accessible for a GeNW of width L, and then the highest-phonon frequency of the system can be approximately determined by evaluating the frequency of optical mode at π/L.

In Fig. 5, the calculated Raman response spectrum of a GeNW with $L = 2.11$ nm is compared with the experimental one [5]. The theoretical results include an imaginary part of energy $\eta = 13$ cm^{-1}, in order to take into account the thermal and size distribution effects, and a weight function proportional to $\exp(-|\omega - \omega_R|/8)$. The inclusion of this weight function is to preserve basic ideas of the momentum selection rule, since in principle only

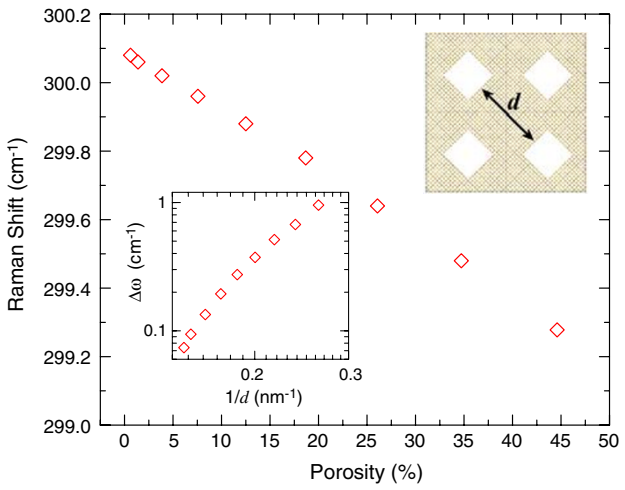

Fig. 3 The Raman shift as a function of the porosity for a fixed supercell of 648 atoms. Inset: $\Delta\omega = \omega_0 - \omega_R$ versus the inverse of partial confinement distance (d), which is illustrated in the upper inset

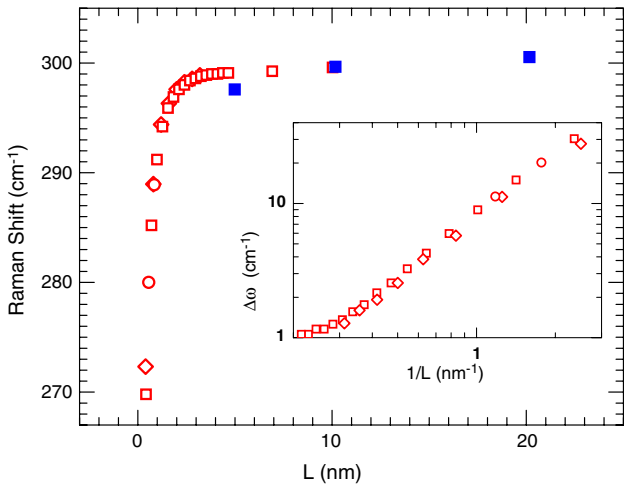

Fig. 4 For Ge nanowires, ω_R is plotted versus the length (L) of cross-sections with square (*open squares*), rhombic (*open rhombus*), and octagonal (*open circles*) form, in comparison to experimental data (*solid square*) obtained from Ref. [14]. Inset: $\Delta\omega = \omega_0 - \omega_R$ as a function of $1/L$ is shown in a log–log plot

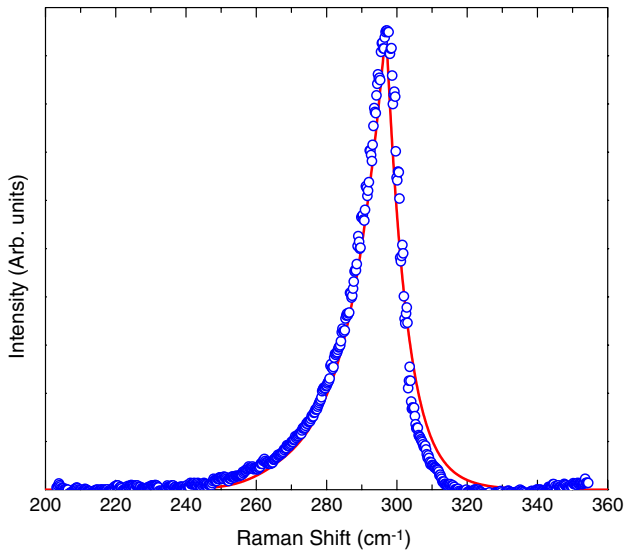

Fig. 5 Raman response of a GeNW with $L = 2.11$ nm (*solid line*) compared with experimental data (*open circles*) from Ref. [5]

Γ-point or infinite-wavelength optical modes are active during the Raman scattering and for a GeNW there are only finite-wavelength modes in x and y directions. In other words, if the Raman selection rule is visualized as a δ-function at Γ-point, it should be broadened for finite-size systems due to the Heisenberg uncertainty principle, i.e., optical modes with a longer wavelength should have a larger participation in the Raman response.

Conclusions

We have presented a microscopic theory to model the Raman scattering in Ge nanostructures. This theory has the advantage of providing a direct relationship between the microscopic structures and the measurable physical quantities. For p-Ge, contrary to the crystallite approach, the supercell model emphasizes the interconnection of the system, which could be relevant for long-range correlated phenomena, such as the Raman scattering. The results show a clear phonon confinement effect on the values of ω_R, and the variation $\Delta\omega$ is in agreement with the effective mass theory. In particular, the Raman response of GeNW is in accordance with experimental data. Regarding to the broadening of Raman peaks, an imaginary part of energy $\eta = 13.0\ \mathrm{cm}^{-1}$ was chosen to include inhomogenous diameters of GeNW, the influence of mechanical stress, as well as laser heating effects [5, 14]. The obtained averaged width $L = 2.11$ nm is smaller than $D = 12.0$ nm estimated in Ref. [5]. This difference could be due to a possible amorphous oxide layer surrounding the surface of GeNW. This study can be extended to other nanostructured semiconductors such as nanotubes.

Acknowledgments This work was partially supported by projects 58938 from CONACyT, 2007045 from SIP-IPN, IN100305 and IN114008 from PAPIIT-UNAM. The supercomputing facilities of DGSCA-UNAM are fully acknowledged.

Appendix A

For tetrahedral structures, the positions of four nearest-neighbor atoms around a central atom located at (0,0,0) are $\vec{R}_1 = (1,1,1)a/4$, $\vec{R}_2 = (-1,-1,1)a/4$, $\vec{R}_3 = (-1,1,-1)a/4$, and $\vec{R}_4 = (1,-1,-1)a/4$, where $a = 5.65$ Å.

From Eq. 3 in "Modeling Raman Scattering", the interaction potential between central atom 0 and atom 1 is

$$V_{0,1} = \frac{\alpha-\beta}{2}\left\{[\mathbf{u}(0)-\mathbf{u}(1)]\cdot\hat{\mathbf{r}}_{0,1}\right\}^2 + \frac{\beta}{2}[\mathbf{u}(0)-\mathbf{u}(1)]^2 \tag{A.1}$$

where $\hat{\mathbf{r}}_{0,1} = \frac{1}{\sqrt{3}}(1,1,1)$ and then, the element xx of the first interaction matrix is given by

$$\phi_{xx}(0,\ 1) = \frac{\partial^2 V_{0,1}}{\partial u_x(0)\ \partial u_x(1)} = -\frac{1}{3}(\alpha+2\beta). \tag{A.2}$$

In a similar way, one can obtain other elements of the matrix. Therefore, the four interaction matrices ϕ_i, bounding the central atom to its nearest-neighbor atom i, can be written as

$$\phi_1 \equiv \phi(0,\ 1) = -\frac{1}{3}\begin{pmatrix} \alpha+2\beta & \alpha-\beta & \alpha-\beta \\ \alpha-\beta & \alpha+2\beta & \alpha-\beta \\ \alpha-\beta & \alpha-\beta & \alpha+2\beta \end{pmatrix}, \tag{A.3}$$

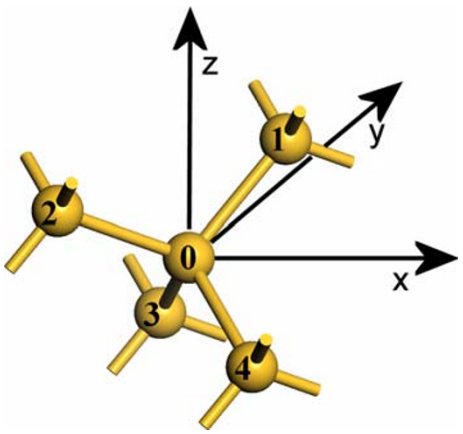

Fig. A1 The positions of four tetrahedral nearest neighbors around a central atom

$$\phi_2 \equiv \phi(0,\ 2) = -\frac{1}{3}\begin{pmatrix} \alpha+2\beta & \alpha-\beta & \beta-\alpha \\ \alpha-\beta & \alpha+2\beta & \beta-\alpha \\ \beta-\alpha & \beta-\alpha & \alpha+2\beta \end{pmatrix}, \tag{A.4}$$

$$\phi_3 \equiv \phi(0,\ 3) = -\frac{1}{3}\begin{pmatrix} \alpha+2\beta & \beta-\alpha & \alpha-\beta \\ \beta-\alpha & \alpha+2\beta & \beta-\alpha \\ \alpha-\beta & \beta-\alpha & \alpha+2\beta \end{pmatrix}, \tag{A.5}$$

and

$$\phi_4 \equiv \phi(0,\ 4) = -\frac{1}{3}\begin{pmatrix} \alpha+2\beta & \beta-\alpha & \beta-\alpha \\ \beta-\alpha & \alpha+2\beta & \alpha-\beta \\ \beta-\alpha & \alpha-\beta & \alpha+2\beta \end{pmatrix}. \tag{A.6}$$

These four interaction matrices ϕ_1, ϕ_2, ϕ_3, and ϕ_4 are indicated in the inset of Fig. 1b. Due to the tetrahedral symmetry it is easy to prove that

$$\phi_s = \phi_1 + \phi_2 + \phi_3 + \phi_4 = -\frac{4}{3}(\alpha-\beta)\mathbf{I}. \tag{A.7}$$

where $\mathbf{I}$ is the identity matrix.

Within the supercell model, the equilibrium positions of atoms i and j can be, respectively, written as $\vec{l}+\vec{b}$ and $\vec{l}'+\vec{b}'$, being $\vec{l}$, $\vec{l}'$ the coordinates of unit cell and $\vec{b}$, $\vec{b}'$ the positions inside the cell. For an eight-atom supercell, the Fourier transform of $\mathbf{\Phi}$ can be written as

$$D_{\mu\mu'}(\vec{b}\vec{b}'|\vec{q}) = \sum_{l,l'} \Phi_{\mu\mu'}(\vec{l}\vec{b};\vec{l}'\vec{b}')\, e^{i\vec{q}\cdot(\vec{l}-\vec{l}')}$$

$$= \begin{pmatrix} \phi_s & 0 & F_4\phi_4 & F_2\phi_2 & F_3\phi_3 & 0 & F_1\phi_1 & 0 \\ 0 & \phi_s & F_1\phi_1 & F_3\phi_3 & F_2\phi_2 & 0 & F_4\phi_4 & 0 \\ F_4^*\phi_4 & F_1^*\phi_1 & \phi_s & 0 & 0 & F_2^*\phi_2 & 0 & F_3^*\phi_3 \\ F_2^*\phi_2 & F_3^*\phi_3 & 0 & \phi_s & 0 & F_4^*\phi_4 & 0 & F_1^*\phi_1 \\ F_3^*\phi_3 & F_2^*\phi_2 & 0 & 0 & \phi_s & F_1^*\phi_1 & 0 & F_4^*\phi_4 \\ 0 & 0 & F_2\phi_2 & F_4\phi_4 & F_1\phi_1 & \phi_s & F_3\phi_3 & 0 \\ F_1^*\phi_1 & F_4^*\phi_4 & 0 & 0 & 0 & F_3^*\phi_3 & \phi_s & F_2^*\phi_2 \\ 0 & 0 & F_3\phi_3 & F_1\phi_1 & F_4\phi_4 & 0 & F_2\phi_2 & \phi_s \end{pmatrix}, \tag{A.8}$$

where the changes of phase related to the phonon wave vector ($\vec{q}$) are given by $F_1 = e^{i\vec{q}\cdot\vec{R}_1}$, $F_2 = e^{i\vec{q}\cdot\vec{R}_2}$, $F_3 = e^{i\vec{q}\cdot\vec{R}_3}$, and $F_4 = e^{i\vec{q}\cdot\vec{R}_4}$. Hence, Eq. 2 can be rewritten as

$$\left[M\omega^2\mathbf{I} - \mathbf{D}(\vec{q})\right]\mathbf{G}(\omega,\ \vec{q}) = \mathbf{I}. \tag{A.9}$$

It is worth to mention that Eq. (A.9) has an associate eigenvalue equation, which leads to the phonon band structure shown in Fig. 1a. Furthermore, the dimension of matrixes involved in Eq. (A.9) is $3N$, N being the number of atoms in the supercell.

References

1. J. Konle, H. Presting, H. Kibbel, Physica E **16**, 596 (2003)
2. C. Fang, H. Föll, J. Carstensen, J. Electroanal. Chem. **589**, 258 (2006)
3. D. Sun, A.E. Riley, A.J. Cadby, E.K. Richman, S.D. Korlann, S.H. Tolbert, Nature **441**, 1126 (2006)
4. G.S. Armatas, M.G. Kanatzidis, Nature **441**, 1122 (2006)
5. R. Jalilian, G.U. Sumanasekera, H. Chandrasekharan, M.K. Sunkara, Phys. Rev. B **74**, 155421 (2006)
6. C. Fang, H. Föll, J. Carstensen, Nano Lett. **6**, 1578 (2006)
7. R. Alben, D. Weaire, J.E. Smith, M.H. Brodsky, Phys. Rev. B **11**, 2275 (1975)
8. R.J. Elliott, J.A. Krumhansl, P.L. Leath, Rev. Mod. Phys. **46**, 465 (1974)
9. C. Wang, R.A. Barrio, Phys. Rev. Lett. **61**, 191 (1988)
10. G.P. Srivastava, *The Physics of Phonons* (Bristol, Adam Hilger, 1990)
11. G. Nilsson, G. Nelin, Phys. Rev. B **3**, 364 (1971)
12. G. Bose, B.B. Tripathi, H.C. Gupta, J. Phys. Chem. Solids **34**, 1867 (1973)
13. E. Finlayson, A. Amezcua-Correa, P.J.A. Sazio, N.F. Baril, J.V. Badding, Appl. Phys. Lett. **90**, 132110 (2007)
14. X. Wang, A. Shakouri, B. Yu, X. Sun, M. Meyyappan, J. Appl. Phys. **102**, 014304 (2007)
15. P. Alfaro, M. Cruz, C. Wang, IEEE Trans. Nanotech **5**, 466 (2006)
16. M. Cruz, C. Wang, M.R. Beltrán, J. Tagüeña-Martínez, Phys. Rev. B **53**, 3827 (1996)